RJC

RASĀYAN ***J. Chem.***
Vol. 18 | No. 4 |1913-1919| October-December | 2025
ISSN: 0974-1496 | e-ISSN: 0976-0083 | CODEN: RJCABP
http://www.rasayanjournal.com
http://www.rasayanjournal.co.in

OPTIMIZING POWER CONVERSION EFFICIENCY OF PEROVSKITE SOLAR CELLS USING DUAL TIO_2-PCBM ELECTRON TRANSPORT LAYERS

G. Purwiandono[1,✉], P. Lestari[2] and F.B. Maziya[2]

[1]Department of Chemistry, Universitas Islam Indonesia, Yogyakarta-55584, Indonesia
[2]Department of Environmental Engineering, Universitas Islam Indonesia, Yogyakarta-55584, Indonesia
✉Corresponding author: gani_purwiandono@uii.ac.id

ABSTRACT

This research utilizes computational modeling to investigate the performance optimization of perovskite solar cells (PSCs) using a dual electron transport layer (ETL) configuration. The architecture under study combines titanium dioxide (TiO_2) and phenyl-C61-butyric acid methyl ester (PCBM) as a bilayer ETL, aiming to improve interfacial alignment and reduce carrier recombination compared to single-layer TiO_2 ETLs. Simulations were carried out using the SCAPS-1D platform, which enabled a detailed evaluation of critical parameters, including defect concentrations, interfacial recombination rates, and operating temperature within a six-layer device structure. The findings revealed a highest power conversion efficiency of 26.667% at the temperature of 290 K. This work contributes to the computational studies on dual-layer ETL designs and provides foundational insights for advancing the development of high-efficiency PSCs.

Keywords: Dual ETL, TiO_2, PCBM, Perovskite Solar Cell, and SCAPS-1D

RASĀYAN *J. Chem.*, Vol. 18, No.4, 2025

INTRODUCTION

Perovskite solar cells (PSCs) are considered the next-generation photovoltaic technology, offering a pathway to achieving higher efficiencies at lower costs compared to traditional silicon-based solar cells.[1,2] These devices are typically designed with an electron transport layer (ETL), a perovskite absorber layer, and a hole transport layer, which plays a critical role in the separation and collection of charges.[3–5] The ETL is a crucial component that is responsible for the extraction of electrons from the perovskite absorber and the blocking of holes to minimize recombination.[6–8] The performance of PSCs is heavily dependent on the characteristics of the ETL.[8] Among the materials, TiO_2 is being extensively used as the ETL due to its favourable band alignment and stability.[9,10] However, the traditional single-layer TiO_2 ETLs often face challenges related to interface defects and restricted electron mobility, which, unfortunately, affect the device performance.[11] A double-layer electron transport layer architecture has emerged as a promising strategy to address these limitations and enhance overall device performance.[8,11] Phenyl-C61-butyric acid methyl ester (PCBM) has been used as an electron acceptor in PSCs.[12] This study aims to address the limitations of traditional single-layer ETLs in PSCs by investigating the potential of a dual-layer configuration using TiO_2 and PCBM. This design allows for the precise adjustment of each layer's properties to enhance electron extraction and transport, improve interfacial contact with the perovskite layer, increase electron mobility, and minimize recombination.[13,14] Layer thicknesses and doping concentrations can be carefully optimized with the assistance of numerical simulations, especially the SCAPS-1D program, which provides a powerful platform for investigating the effects of changing ETL parameters on the device performance.[15] In 2023, Banoth *et al.* investigated the experimental studies that demonstrate the fabrication of stacked TiO_2 layers with precisely engineered thicknesses and properties can enhance energy band alignment and decrease interfacial recombination.[16] Despite these improvements, systematic computational analyses quantitatively assessing the effects of double ETLs on PSC performance remain limited.[17,18] The objective of this study is to address this knowledge gap by utilizing SCAPS-1D simulations to comprehensively investigate the impact of changing critical parameters, such as interface recombination velocities and defect densities, under varying temperature conditions in a double-layer ETL

http://doi.org/10.31788/RJC.2025.1849402

structure. This method offers critical insights that will assist in the design and optimization of high-performance perovskite solar cells.

EXPERIMENTAL

Simulation Device Architecture

The numerical simulations were performed using the SCAPS-1D simulation software (version 3.3.09).[19,20] The simulation device structure consisted of six layers arranged in the following order from the front contact to the back contact: FTO layer, TiO_2, PCBM, MASnI3, P3HT, Spiro-OMeTAD, and Au, as shown in Fig.-1. The simulation temperature was varied between 270 K and 350 K, and focused on defect concentrations, interfacial recombination rates, and power conversion efficiency.

Layer Parameters

The specific thicknesses and key material parameters for each layer, along with interface properties, were defined in Table-1. The main performance indicators of PSCs are the fill factor (FF) and power conversion efficiency (PCE), which are calculated using formulas 1 and 2.

$$FF = \frac{V_{mp} \cdot J_{mp}}{V_{oc} \cdot J_{sc}} \quad (1)$$

$$PCE = \frac{V_{oc} \cdot J_{cs} \cdot FF}{P_{in}} \quad (2)$$

In which V_{mp} and J_{mp} represent the voltage and current density at the maximum power point, while V_{oc}, J_{sc}, and P_{in} refer to the open-circuit voltage, short-circuit current density, and the input power from the incident light, respectively.

Table-1: Simulation Parameters for the Perovskite Layers

Parameters	FTO[21]	TiO_2[22]	PCBM[23]	MASnI3[19]	P3HT[24]	Spiro-OMeTAD[22]
Thickness (nm)	500	30	50	600	50	200
Bandgap (eV)	3.5	3.2	2.0	1.3	1.7	2.88
Electron affinity (eV)	4.0	4.0	3.9	4.2	3.5	2.05
Dielectric permittivity (ε_r)	9.0	9.0	3.9	10	3.0	3.0
DOS CB, N_c (cm^{-3})	2.2×10^{18}	2.2×10^{18}	2.5×10^{21}	1.0×10^{18}	2.0×10^{21}	2.2×10^{18}
DOS VB, N_v (cm^{-3})	1.8×10^{19}	1.8×10^{19}	2.5×10^{21}	1.0×10^{18}	2.0×10^{21}	1.8×10^{19}
Electron mobility, μ_n ($cm^2\ V^{-1}s^{-1}$)	20	20	0.2	1.6	1.8×10^{-3}	2.0×10^{-4}
Hole mobility, μ_h ($cm^2\ V^{-1}s^{-1}$)	10	10	0.2	1.6	1.8×10^{-2}	2.0×10^{-4}
Acceptor density, N_A (cm^{-3})	0	0	0	1.0×10^{15}	1.0×10^{18}	2.0×10^{19}
Donor density, N_D (cm^{-3})	2.0×10^{19}	9.0×10^{16}	2.93×10^{17}	0	0	0

Alternating current (A—C) Characterization allows for the collection of complex impedance data across a range of frequencies. These measurements can be performed under various conditions, such as different applied biases, temperature variations, and simulated lighting environments. All simulations were performed under standard AM1.5G illumination incident from the front, with a broad wavelength range of 200 nm to 4000 nm.[25,26] The primary simulation sweep involved varying the ambient temperature from 270 K to 350 K.[17,27]

RESULTS AND DISCUSSION

Comparative Performance of Double ETLs Perovskite Solar Cell

The simulation results clearly demonstrated that the double ETL significantly enhanced the overall photovoltaic performance of the perovskite solar cells compared to a conventional single ETL configuration, as shown in Table-2. The results highlighted a significant improvement in power conversion

efficiency upon employing a double-layer ETL, with the efficiency rising from 17.885% in the single-layer design to an enhanced 27.167% at a temperature of 300 K.

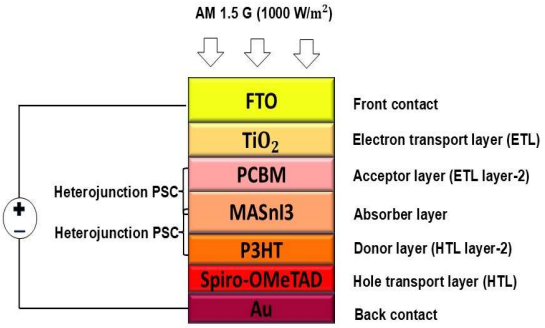

Fig.-1: Device Structure of Six-Layer Dual ETL and HTL Perovskite Solar Cell

This improvement suggested the capability of the double-layer ETL to facilitate superior charge separation and transport. The performance of perovskite solar cells was significantly affected by the architecture of the ETL, where modifications such as the introduction of double-layer structures markedly altered device characteristics.[26,28]

Table-2: Enhancement in Photovoltaic Parameters: a Comparison between Single and Double ETL Architectures

ETL	Temperature (K)	Efficiency (%)	V_{OC} (V)	J_{SC} (mA/cm^2)	FF (%)
Single ETL	280	18.960	0.694	33.344	81.942
	300	17.885	0.664	33.345	80.812
	320	16.798	0.633	33.347	79.592
	340	15.705	0.602	33.350	78.248
Double ETL	280	27.667	1.013	33.359	81.841
	300	27.167	1.007	33.360	80.873
	320	26.661	1.001	33.361	79.914
	340	26.151	0.993	33.364	78.962

Furthermore, the efficiency trend for the single ETL configuration indicated that its efficiency decreased with increasing temperature, as evidenced by a drop from 18.960% at 280 K to 15.705% at 340 K, as shown in Table-2. In contrast, the double ETL configuration significantly enhanced overall photovoltaic performance, achieving an efficiency of 27.667% at 280 K. This significant improvement can be attributed to the double-layer ETL's capability to facilitate superior charge separation and transport. Specifically, it reduced non-radiative recombination losses at the ETL/perovskite interface and within the ETL layers themselves.[8,11] The presence of two layers created a more favourable band alignment that facilitated electron extraction while more effectively blocking holes, thereby suppressing recombination pathways.[29,30] This led to an increase in open-circuit voltage, short-circuit current density, and fill factor.[31] Specifically, the first TiO_2 layer acted as an initial electron extraction interface, while the second layer served as an effective buffer, smoothing energy band discontinuities and providing a better interface with the transparent conducting oxide, ultimately reducing interface defect states and lowering recombination velocities.

J—V Characterization

To further evaluate the impact of temperature on PSC's device, Fig.-2 presents the current density-voltage characteristics of perovskite solar cells over a temperature range of 270 K to 350 K. These curves consistently showed current density behaviour dependent on voltage, initiating at a certain current value when voltage was zero and decreasing to zero near the open-circuit voltage. A notable initial plateau was observed in each curve, indicating a relatively stable current density before its decline, which is typical for PSC J—V profiles. Although a distinct peak in current density with respect to temperature was not depicted, the overall device performance, including metrics extracted from the J—V curves, clearly diminished as temperatures exceeded 280 K. This trend aligns well with the general understanding that elevated temperatures typically compromise PSC efficiency. Specifically, higher temperatures exacerbate carrier

recombination and introduce other resistive losses, collectively contributing to the performance degradation. Notably, PSCs exhibited their peak performance at 280 K, evidenced by a greater current output at specific voltages and attainment of maximum efficiency. Consequently, sustaining the PSCs at or near this ideal temperature is vital for realizing substantial performance gains. Through this J—V analysis, a critical understanding of PSC operation across varied environmental temperatures. In summary, gaining insight into temperature behaviour is essential for optimizing the performance of PSC and enhancing their energy conversion capabilities.[32]

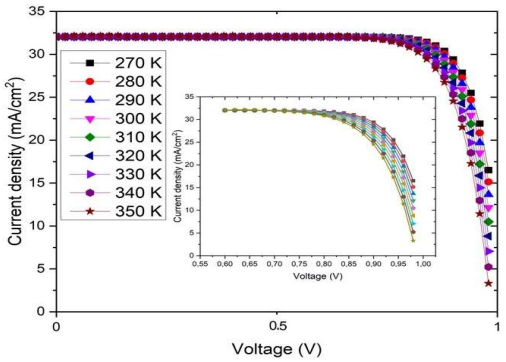

Fig.-2: J—V curve of PSCs in different temperatures

Moreover, the thermal sensitivity of PSCs is evident in their response to variations in V_{OC} and J_{SC}, as depicted in Fig.-3(a). A consistent linear decline in V_{OC} with increasing temperature is observed, attributed to bandgap narrowing and elevated carrier recombination. In contrast, J_{SC} exhibits a biphasic response-initially increasing from 270 K to 290 K due to improved charge transport, then declining beyond 290 K due to intensifying recombination and resistive losses. The fill factor (FF) exhibits a maximum near 290 K, indicating favorable charge extraction under moderate thermal conditions. However, a decline is observed at elevated temperatures, likely attributed to heat-induced degradation mechanisms. Similarly, the power conversion efficiency (PCE) reaches its highest value at 290 K, signifying a thermodynamic sweet spot where V_{OC}, J_{SC}, and FF are optimally aligned, as shown in Fig.-3(b). Efficiency deteriorates significantly at temperatures above this threshold, driven by compounded loss pathways.

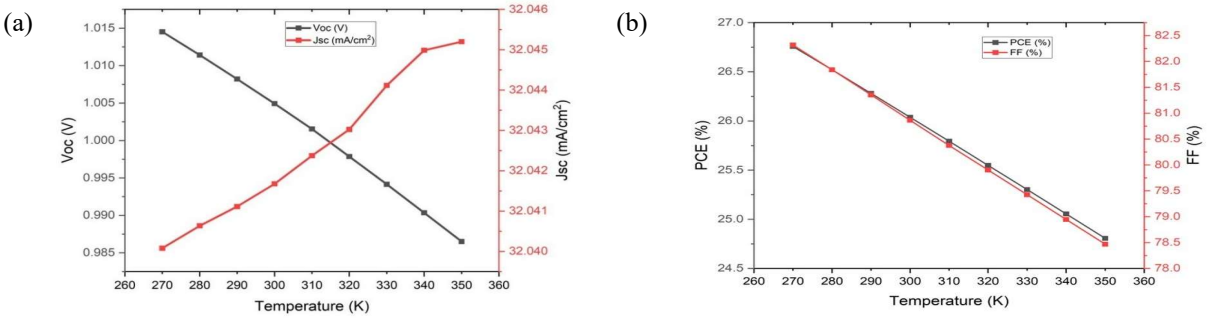

Fig.-3: Temperature effect on Parameters of the PSC (a) V_{OC} and J_{SC} (b) FF% and PCE%

Collectively, these observations highlight the critical importance of thermal control and the advancement of materials and device configurations capable of withstanding thermal stress. Recognizing 290 K as a temperature of peak photovoltaic performance provides a strategic benchmark for improving PSC designs. Enhancing stability and performance through improved heat management and interface optimization could pave the way for more reliable operation in practical settings.

A—C Characterization

To further elucidate the influence of temperature on the electrical behaviour of PSCs, Nyquist diagrams, as depicted in Fig.-4(a), consistently demonstrated a uniform response of the devices across all temperature conditions. The presence of a solitary semicircle in these diagrams indicated a relatively straightforward

equivalent circuit model for the cell's impedance. Notably, an increase in temperature from 270 K to 290 K resulted in an expansion of the semicircle diameter, signaling a corresponding increase in overall impedance. This phenomenon may be attributed to thermally induced changes in interfacial resistance or altered charge carrier mobility. However, a contrasting trend was observed beyond 290 K. As the temperature continued to rise, the semicircle diameter began to diminish, indicating a decrease in impedance. This atypical reduction suggests a transition in the dominant charge transport or recombination mechanisms, potentially driven by enhanced ion migration or temperature-induced alterations in material properties. The equivalent circuit model presented in Fig.-4(b) offers a useful framework to interpret these temperature-dependent impedance behaviors and their implications for PSC performance. In addition to the Nyquist plots, Fig.-4(b) also provides Bode diagram representations of impedance spectra across the temperature range of 270 K to 350 K. These diagrams, plotting the negative imaginary component of impedance ($-Z''$) against frequency on a logarithmic scale, reveal distinct peaks corresponding to specific relaxation processes within the PSCs. As the temperature increased, the consistent shift of these peaks toward higher frequencies suggested the presence of a thermally activated relaxation mechanism. Furthermore, a notable decrease in peak amplitude was observed across this temperature range, implying a reduction in charge carrier recombination resistance or ionic movement constraints. This trend is consistent with prior studies in semiconducting materials, which show improved charge mobility at elevated temperatures. Supporting this, Krishnaiah *et al.*[33] reported a similar thermally induced photovoltaic absorber in $Cs_2AgBi_2I_9$. Moreover, at the upper temperature limits of this range, the impedance peaks exhibited broader shapes, indicating a wider distribution of relaxation times. This broadening may reflect increased material heterogeneity or frequency dispersion effects, which have been previously discussed by Alharshan *et al.*[34]

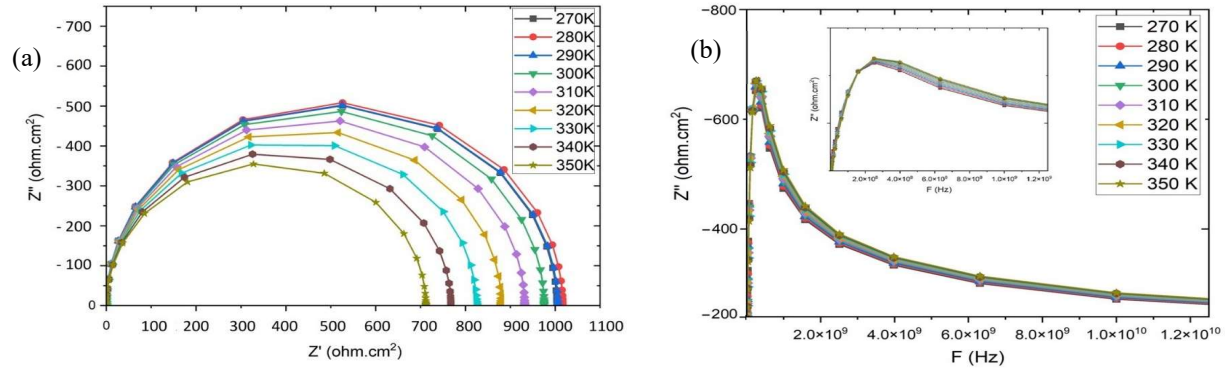

Fig.-4: Impedance Spectra in the Range of Temperature 270 K ─ 350 K, depicted as (a) Nyquist Diagrams and (b) Bode Diagrams

Although the reduced impedance at elevated temperatures may initially appear advantageous for charge transport, it must be interpreted with caution. Critically, as emphasized by Zhu *et al.,* elevated temperatures can jeopardize the structural stability of perovskite materials, thereby posing long-term reliability challenges.[35] Therefore, while thermal activation can improve transport properties, it also risks accelerating degradation processes. In light of these observations, it becomes essential to develop strategies that can mitigate thermally induced degradation while preserving or enhancing charge transport. Tailoring advanced architectures, such as the implementation of double electron transport layers, may offer a promising pathway to improving both the efficiency and thermal resilience of PSCs.

CONCLUSION

In this study, we explored how temperature variations influence the behavior and performance of a double-layer electron transport design using TiO_2 and PCBM perovskite solar cells (PSCs) in their electrical characteristics. Our findings indicate that the cells operate most efficiently at 290 K, achieving a peak power conversion efficiency of 26.67%. When the temperature rises beyond this point, efficiency drops noticeably-largely due to increased recombination events and higher resistance, which confirms the devices' thermal sensitivity. These results suggest that future improvements in PSCs should focus on refining electron transport layers and integrating effective heat management systems. Such efforts are likely to be

key in making perovskite solar cells both efficient and reliable enough for widespread use in real-world environments.

ACKNOWLEDGMENTS

This study is supported by the Indonesian Directorate of Research, Technology, and Community Service under grant number 0459/E5/PG.02.00/2024, with contract number 0609.1/LL5-INT/AL.04/2024.

CONFLICT OF INTERESTS

The authors declare that there is no conflict of interest.

AUTHOR CONTRIBUTIONS

The present work is related to *SDG-7: Affordable and clean energy*. All the authors contributed significantly to this manuscript, participated in reviewing/editing and approved the final draft for publication. The research profile of the authors can be verified from their ORCID ids, given below:

Gani Purwiandono https://orcid.org/my-orcid?orcid=0000-0003-2240-7832
Puji Lestari https://orcid.org/0000-0002-6274-1176
Fina Binazir Maziya https://orcid.org/0000-0002-7450-8291

REFERENCES

1. G.G. Njema and J.K. Kibet, *International Journal of Photoenergy,* **3801813,** (2023), https://doi.org/10.1155/2023/3801813
2. M.J. Talukder, M. Akteruzzaman, Z. Hasan, and E. Haque, *The American Journal of Advanced Technology and Engineering Solutions,* **1**, 201(2025), https://doi.org/10.63125/5amnvb37
3. S. Foo, M. Thambidurai, P. Senthil Kumar, R. Yuvakkumar, Y. Huang, and C. Dang, *International Journal of Energy Research,* **46**, 21441(2022), https://doi.org/10.1002/er.7958
4. L. Lin, T.W. Jones, T.C. Yang, N.W. Duffy, J. Li, L. Zhao, B. Chi, X. Wang, and G.J. Wilson, *Advanced Functional Materials,* **31**, 2008300(2021), https://doi.org/10.1002/adfm.202008300
5. M. Cheng, C. Zuo, Y. Wu, Z. Li, B. Xu, Y. Hua, and L. Ding, *Science Bulletin,* **65**, 1237(2020), https://doi.org/10.1016/j.scib.2020.04.021
6. H. Ferhati, F. Abdel Malek, and F. Djeffal, *Solar Energy,* **262**, 111805(2023), https://doi.org/10.1016/j.solener.2023.111805
7. A. Ahmed, K. Riaz, H. Mehmood, T. Tauqeer, and Z. Ahmad, *Optical Materials,* **105**, 109897(2020), https://doi.org/10.1016/j.optmat.2020.109897
8. H. Pan, X. Zhao, X. Gong, H. Li, N.H. Ladi, X.L. Zhang, W. Huang, S. Ahmad, L. Ding, and Y. Shen, *Materials Horizons,* **7**, 2276(2020), https://doi.org/10.1039/D0MH00586J
9. Q. Fatima, A.A. Haidry, H. Zhang, A. El Jery, and M. Aldrdery, *Materials Today Sustainability,* **100857**(2024), https://doi.org/10.4236/mnsms.2024.144006
10. M.M. Tavakoli, P. Yadav, R. Tavakoli, and J. Kong, *Advanced Energy Materials,* **8**, 1800794(2018), https://doi.org/10.1002/aenm.201800794
11. L. Zang, C. Zhao, X. Hu, J. Tao, S. Chen, and J. Chu, *Small,* **20**, 2400807(2024), https://doi.org/10.1002/smll.202400807
12. M.N. Uddin and P. Afrin, *Optik*, **302**, 171691(2024), https://doi.org/10.1016/j.ijleo.2024.171691
13. M.K. Hossain, D.P. Samajdar, R.C. Das, A.A. Arnab, M.F. Rahman, M.H.K. Rubel, M.R. Islam, H. Bencherif, R. Pandey, and J. Madan, *Energy & Fuels,* **37**, 3957(2023), https://doi.org/10.1039/D3RA02485G
14. Y. Gao, Y. Wu, Y. Liu, C. Chen, X. Shen, X. Bai, Z. Shi, W.W. Yu, Q. Dai, and Y. Zhang, *Solar RRL,* **3**, 1900314(2019), https://doi.org/10.1002/solr.201900314
15. M.S. Islam, M.T. Islam, S. Sarker, H. Al Jame, S.S. Nishat, M.R. Jani, A. Rauf, S. Ahsan, K.M. Shorowordi, and H. Efstathiadis, *ACS Omega,* **7**, 22263(2022),

https://doi.org/10.1021/acsomega.2c01076
16. R. Banoth, P.V.R. Shekar, C. V Ramana, and K. Kumari, *Colloids and Surfaces A: Physicochemical and Engineering Aspects,* **676**, 132075(2023), https://doi.org/10.1016/j.colsurfa.2023.132075
17. M.I. Hossain, P. Chelvanathan, A. Khandakar, K. Thomas, A. Rahman, and S. Mansour, *Scientific Reports,* **14**, 12984(2024), https://doi.org/10.1038/s41598-024-62487-0
18. K. Gupta, O.P. Thakur, and M. Kumar, *Optical Materials,* **150**, 115125(2024), https://doi.org/10.1016/j.optmat.2024.115125
19. F. Arif, M. Aamir, A. Shuja, M. Shahiduzzaman, and J. Akhtar, *Results in Optics*, **14**, 100595(2024), https://doi.org/10.1016/j.rio.2023.100595
20. P. Van Duong, P.T.P. Le, and C.N.T. Kim, *Physica Scripta,* **100**, 45909(2025), https://doi.org/10.1088/1402-4896/adba1c
21. Y. Chen, Y. Lei, Y. Li, Y. Yu, J. Cai, M.-H. Chiu, R. Rao, Y. Gu, C. Wang, and W. Choi, *Nature,* **577**, 209(2020), https://doi.org/10.1038/s41586-019-1868-x
22. E. Danladi, P.M. Gyuk, N.N. Tasie, A.C. Egbugha, D. Behera, I. Hossain, I.M. Bagudo, M.L. Madugu, and J.T. Ikyumbur, *Heliyon,* **9(6)**, e16838(2023), https://doi.org/10.1016/j.heliyon.2023.e16838
23. A.S. Alali, M. Oduncuoglu, and F. Touati, *Nanomaterials,* **14**, 1146(2024), https://doi.org/10.3390/nano14131146
24. H. Zhang, Z.-N. Ng, C.C. Kang, J.D. Tan, M. Ariannejad, M.A.S. Bhuiyan, and K.-Y. Chan, *Energy Reports,* **12**, 2707(2024), https://doi.org/10.1016/j.egyr.2024.08.045
25. M.M. Hassan, Z.S. Ismail, E.M. Hashem, R. Ghannam, and S.O. Abdellatif, IEEE *Journal of Photovoltaics,* **11**, 1222(2021), https://doi.org/10.1109/JPHOTOV.2021.3086443
26. H. Zhang, Z.-N. Ng, C.C. Kang, J.D. Tan, M. Ariannejad, M.A.S. Bhuiyan, and K.-Y. Chan, *Energy Reports,* **12**, 2707(2024), https://doi.org/10.1016/j.egyr.2024.08.045
27. E. Danladi, M. Kashif, M. Ouladsmane, I. Hossain, A.C. Egbugha, J.O. Alao, C.U. Achem, N.N. Tasie, O.S. Aremo, and A.M. Umar, *Optik*, **291**, 171325(2023), https://doi.org/10.1016/j.ijleo.2023.17132
28. M.F.M. Noh, C.H. Teh, R. Daik, E.L. Lim, C.C. Yap, M.A. Ibrahim, N.A. Ludin, A.R. bin Mohd Yusoff, J. Jang, and M.A.M. Teridi, *Journal of Materials Chemistry C,* **6**, 682(2018), https://doi.org/10.1039/C8NA00317C
29. S. Chen, J. Li, J. Bai, L. Xia, Y. Zhang, L. Li, Q. Xu, and B. Zhou, *Applied Catalysis B: Environmental,* **237**, 175(2018), https://doi.org/10.1016/j.apcatb.2018.05.068
30. C. Ding, Y. Zhang, F. Liu, Y. Kitabatake, S. Hayase, T. Toyoda, K. Yoshino, T. Minemoto, K. Katayama, and Q. Shen, *Nano Energy,* **53**, 17(2018), https://doi.org/10.1016/j.nanoen.2018.08.031
31. J. Wang, *EcoMat,* **4**, e12263(2022), https://doi.org/10.1002/eom2.12263
32. H. Liu, W. Shuai, Z. Yao, J. Xuan, M. Ni, G. Xiao, and H. Xu, *Applied Energy,* **377**, 124610(2025), https://doi.org/10.1016/j.apenergy.2024.124610
33. M. Krishnaiah, K. Singh, S. Monga, A. Tripathi, S. Karmakar, R. Kumar, C. Tyrpenou, G. Volonakis, D. Manna, and P. Mäkinen, *Advanced Energy Materials,* **15**, 2404547(2025), https://doi.org/10.1002/aenm.202404547
34. G.A. Alharshan, H.M. Gomaa, M.A.M. Uosif, and E.R. Shaaban, *Ionics*, **31**, 6741(2025), https://doi.org/10.1007/s11581-025-06382-2
35. H. Zhu, S. Teale, M.N. Lintangpradipto, S. Mahesh, B. Chen, M.D. McGehee, E.H. Sargent, and O.M. Bakr, *Nature Reviews Materials,* **8**, 569(2023), https://doi.org/10.1038/s41578-023-00582-w

[RJC-9402/2025]